Journal of the Ceramic Society of Japan 118 [8] 717-721 2010 Paper

Piezoelectric anomalies at the ferroelastic phase transitions of lead-free tungsten bronze ferroelectrics

Takayuki WATANABE,† Jumpei HAYASHI, Takanori MATSUDA, Toshihiro IFUKU, Bong-Yeon LEE,* Takashi IIJIMA,* Hiroshi FUNAKUBO, Houzhona YU*** and Nobuhiro KUMADA*****

Corporate R&D Headquarters, CANON INC., 3–30–2 Shimomaruko, Ohta-ku, Tokyo 146–8501
*Research Center for Hydrogen Industrial Use and Storage, National Institute of Advanced Industrial Science and Technology (AIST), AIST Tsukuba Central 5, Tsukuba 305–8565
**Department of Innovative and Engineered Materials, Tokyo Institute of Technology, 4259 Nagatsuta-cho, Midori-ku, Yokohama 226–8502
***Department of Research Interdisciplinary Graduate School of Medicine and Engineering, University of Yamanashi, 7 Miyamae-cho, Ko-fu, Yamanashi 400–8511

This paper reports on the piezoelectric anomalies at the temperature or composition-induced ferroelastic phase transitions of tungsten bronze ferroelectrics. First, the temperature-dependent piezoelectric properties of $Sr_{1.9}Ca_{0.1}NaNb_5O_{15}$ (SCNN) ceramics were characterized using a resonance/anti-resonance method. SCNN has a ferroelastic phase transition manifested by a broad dielectric peak in the temperature range of −60°C to 20°C. The electromechanical coupling factor and elastic compliance showed the maximum at −40°C, increasing the transverse piezoelectric constant (d_{31}) by 38% compared with the room temperature value. Tungsten bronze ferroelectrics follow a trade-off relationship between the longitudinal piezoelectric constant (d_{33}) and the Curie temperature, while SCNN deviates significantly from the trend curve. This deviation is attributed to the ferroelastic phase transition close to room temperature.

Second, the ferroelastic phase transition was investigated for epitaxial films of $(1-x)(Sr_3Ba_2)Nb_{10}O_{30}$–$xBa_4Bi_{2/3}Nb_{10}O_{30}$ as a function of the composition. A careful structural analysis by X-ray diffraction revealed that there is a ferroelastic phase boundary between tetragonal and orthorhombic crystals at $x = 0.06$–0.3. The electric field-induced strain and the relative dielectric constants characterized at 80 K for the epitaxial films increased in the vicinity of the phase boundary composition. These results suggest that engineering the ferroelastic phase transition is an approach to improving the piezoelectric properties of lead-free tungsten bronze ferroelectrics.

Key-words : Lead-free, Piezoelectricity, Ferroelastic phase transition, Tungsten bronze, Epitaxial films

[Received April 19, 2010; Accepted June 17, 2010]

1. Introduction

In perovskite ferroelectrics, an exceptionally large piezoresponse at the morphotropic phase boundary (MPB) has been widely reported,[1] and this outstanding piezoelectric performance is attributed to the high orientational diversity of the spontaneous polarization (P_s) achieved at the MPB.[2] Tungsten bronze ferroelectrics are also known for the MPB,[3] and tetragonal and orthorhombic crystals coexist at the phase boundary.[4] The phase transitions in tungsten bronze ferroelectrics are classified into two types in terms of the orientational diversity of the P_s. One phase transition has a high degree of freedom of the P_s orientation, that is, $[001]_{tet}$ and $[100]/[010]_{ortho}$, while the other phase transition takes only one P_s orientation, $[001]_{tet/ortho}$. This is because the P_s of the orthorhombic tungsten bronze ferroelectrics can be oriented along either $[001]_{ortho}$ or $[100]/[010]_{ortho}$ depending upon the chemical composition, while that of tetragonal tungsten bronze ferroelectrics commonly lies along $[001]_{tet}$. Only lead-rich orthorhombic tungsten bronze ferroelectrics, such as $PbNb_2O_6$ and $Pb_2KNb_5O_{15}$, have the P_s along $[100]/[010]_{ortho}$,[5] while other orthorhombic tungsten bronze ferroelectrics are along $[001]_{ortho}$.

Actually, the former phase transition, which has a high orientational diversity of the P_s, contributes to significantly improved piezoelectric properties, as can be seen for $(Pb_{1-x}Ba_x)Nb_2O_6$ ($x = 0.37$ for the MPB).[5] On the other hand, excellent piezoelectric performance may not be expected for the latter phase transition, because the P_s orientation is kept parallel to $[001]_{tet/ortho}$ over the phase transition. However, there is a potential to improve the piezoelectric properties at the phase transition while retaining the P_s orientation.

The phase transition between tetragonal and orthorhombic crystals will be a ferroelastic phase transition, since the tetragonal and orthorhombic tungsten bronze crystals are paraelastic and ferroelastic, respectively.[6] In principle, the elastic compliance of the crystal diverges at the ferroelastic phase transition, and in fact an elastic anomaly at the phase transition was detected.[7] Since the piezoelectric coefficient is a function of the elastic compliance, a piezoelectric anomaly will occur at the ferroelastic phase transition. For example, a transverse dielectric constant (d_{31}) measured on applying an electric field parallel to the poling field is expressed as $d_{31} = k_{31} \cdot (\varepsilon_{33}^{T} \cdot s_{11}^{E})^{0.5}$, where k_{31} is the transverse electromechanical coupling factor; ε_{33}^{T} is the longitudinal dielectric constant at constant stress; and s_{11}^{E} is the transverse elastic compliance for a transverse stress at constant electric field. This equation indicates that the diverging elastic

† Corresponding author: T. Watanabe; E-mail: watanabe.takayuki781@canon.co.jp

compliance acts to increase the piezoelectric constant at the ferroelastic phase transition.

In addition, the electromechanical coupling factor is a function of the elastic compliances as expressed $k_{31}{}^2 = (s_{11}{}^E - s_{11}{}^D)/s_{11}{}^E$, where $s_{11}{}^D$ is the transverse elastic compliance under constant electric displacement. This equation indicates that k_{31} is enhanced if $s_{11}{}^E$ increases more than $s_{11}{}^D$ at the ferroelastic phase transition. Although the phase transitions between lead-free tungsten bronze ferroelectrics do not have the high spatial diversity of the P_s orientation, there is great potential to improve the piezoelectric performance by utilizing the elastic anomaly at the ferroelastic phase transition.

The temperature-induced ferroelastic phase transition, which often manifests itself as the dielectric peak, has been reported for some tungsten bronze materials.[8)–11)] However, the piezoelectric behavior in the vicinity of the transition temperature is rarely reported. In this paper, the lead-free ferroelastic phase transition is mainly discussed. We prepared a typical tungsten bronze crystal, $Sr_{1.9}Ca_{0.1}NaNb_5O_{15}$ (SCNN), which varies from paraelectric/paraelastic tetragonal above the Curie temperature (T_C) to ferroelectric/paraelastic tetragonal and ferroelectric/ferroelastic orthorhombic crystals as the temperature falls,[8)] and probed the piezoelectric behavior in the vicinity of the already known ferroelastic phase transition temperature. In addition, epitaxial films of solid solutions between the tetragonal $(Sr_3Ba_2)Nb_{10}O_{30}$ [SBN] and orthorhombic $Ba_4Bi_{2/3}Nb_{10}O_{30}$ (BBN) phases were grown, and the crystal structure and the piezoresponse were recorded as a function of the composition. Since high quality epitaxial films give a simple, well-separated, and intense X-ray diffraction pattern in contrast to a complex and overlapped powder pattern, they are particularly convenient for tracing the slight changes that occur in the complex crystal structure at the phase transition.

2. Experimental

SCNN ceramics were prepared by conventional solid state sintering. $SrCO_3$, $CaCO_3$, Na_2CO_3, and Nb_2O_5 powders with purities of more than 99% were used as the starting materials. The starting materials were mixed and dry-milled for 12 h and calcined at 1150°C for 6 h. The calcined powder was pressed into pellets with 3 wt% polyvinyl butyral as a binder. The pellets were sintered at 1300–1350°C for 6 h in air and ground down to a thickness of about 1 mm, and polished. The obtained SCNN ceramics consisted of a single tungsten bronze phase with a relative density of 93–97%. Gold electrodes were deposited onto both sides by dc-sputtering, and the electroded specimens were cut into a rectangular shape with a lateral dimension of 2.5×10 mm. These test pieces were poled in an oil bath kept at 200°C for 30 min and cooled down to room temperature under a 20 kV/cm dc field for resonance–antiresonance measurement with an HP4194A impedance analyzer.

Epitaxial films of solid solutions between tetragonal $(Sr_3Ba_2)Nb_{10}O_{30}$ (SBN, $a = b = 1.246$ and $c = 0.3938$ nm)[13)] and orthorhombic $Ba_4Bi_{2/3}Nb_{10}O_{30}$ (BBN, $a = 1.768$, $b = 1.774$, and $c = 0.795$ nm),[14)] $(1-x)$SBN–xBBN, were grown using the rf-sputtering method on La-doped (111)$SrTiO_3$ single crystal substrates at 700–840°C. The P_s axis is parallel to [001] for both SBN and BBN. $SrCO_3$, $BaCO_3$, Bi_2O_3, and Nb_2O_5 powders were mixed and pressed into a 2-inch disc shape to be used as the target. Ar and O_2 gases were flown with a fixed ratio of $Ar/O_2 = 20/1$, and the chamber pressure was set at 0.50 Pa. The film thickness was adjusted to about 1 μm. Circular platinum top electrodes 100 μm in diameter were deposited by dc-sputtering method on the films using a shadow mask. A vacuum chamber equipped with a temperature control stage, quartz windows for a single laser Doppler interferometer, and conductive probes was set up for simultaneously recording the hysteresis loops of the strain and polarization as a function of an external electric field at various temperatures.

The structural properties were analyzed using an X-ray diffractometer (PANalytical, X'pert Pro MRD) equipped with a two bounce hybrid monochromator. For the epitaxial films in particular, X-ray polefigure measurements and asymmetric reflection measurements were performed to analyze the crystal structure in detail. For measurements other than the polefigure, a monochromatic X-ray beam was used. Since the orthorhombic and tetragonal crystals have different unit cell settings,[15)] the crystal system used for describing the crystal orientation and the diffraction index are noted by superscripts, as appropriate.

3. Results and discussions

3.1 Temperature-induced ferroelastic phase transition

Figure 1(a) indicates the relative dielectric constants of non-poled SCNN ceramics measured on heating the sample. In agreement with previous studies,[10),11)] a diffused dielectric peak around −20–0°C was observed, which is explained by the ferroelastic phase transition, as well as a relatively sharp

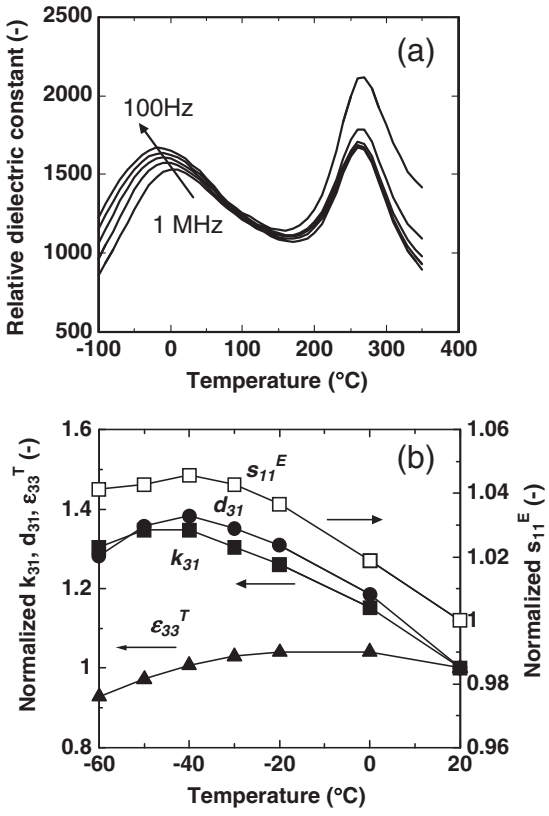

Fig. 1. (a) Relative dielectric constant of a non-poled $Sr_{1.9}Ca_{0.1}NaNb_5O_{15}$ ceramic measured with a 500 mV ac field with frequencies of 100, 1k, 10k, 100k, and 1M Hz; and (b) transverse piezoelectric constant (d_{31}), transverse electromechanical coupling factor (k_{31}), and elastic compliance at constant electric field ($s_{11}{}^E$) characterized for a poled rectangular $Sr_{1.9}Ca_{0.1}NaNb_5O_{15}$ ceramic specimen using a resonance–antiresonance method. In the figure, the longitudinal dielectric constant at constant stress ($\varepsilon_{33}{}^T$) measured at 1 kHz are also shown. The d_{31}, k_{31}, $s_{11}{}^E$, and $\varepsilon_{33}{}^T$ were normalized for the values at 20°C.

dielectric peak at 260–270°C for the T_C. The relative dielectric constant at 1 kHz (ε_r) and the longitudinal piezoelectric constant (d_{33}) measured with a Berlincourt d_{33} meter were 1400 and 80 pC/N. These values are almost identical to those reported in a previous study.[12] The values of d_{31}, k_{31}, and s_{11}^E measured for a poled rectangular SCNN specimen using the resonance–antiresonance method at room temperature were 10 pC/N, 0.055, and 7.9×10^{-12} m^2/N, respectively. Figure 1(b) depicts d_{31}, k_{31}, and s_{11}^E, which were characterized on cooling the specimen from 20°C down to −60°C and normalized by the room temperature values. In the figure, normalized ε_{33}^T measured with a 1 kHz small ac field is also displayed. As expected, s_{11}^E increased as the temperature falls due to the ferroelastic phase transition, and the top value at −40°C was 4.6% larger than the room temperature value. It is particularly worth nothing that k_{31} increased by 35% with a similar temperature dependence to s_{11}^E, reaching a maximum at −40°C. According to the equation, $k_{31}^2 = (s_{11}^E - s_{11}^D)/s_{11}^E$, the present results imply that s_{11}^E increased at the ferroelastic phase transition more than s_{11}^D, so that k_{31} improved. We calculated s_{11}^D using k_{31} and s_{11}^E shown in Fig. 1(b), and found that s_{11}^D had a similar temperature dependence to that of s_{11}^E, while the gain of s_{11}^D at −40°C compared to the room temperature value was 4.4%, less than 4.6% for s_{11}^E. At the ferroelastic phase transition, s_{11}^E increased at a relatively high rate to s_{11}^D, so that k_{31} was improved at the phase transition. In this study, k_{31}, s_{11}^E, and ε_{33}^T increased in the vicinity of the ferroelastic phase transition at −40°C, and eventually d_{31} was enhanced by 38% compared with the room temperature value.

Interestingly, s_{11}^E, k_{31}, and d_{31} reached their maximum at −40°C, which is significantly below the temperature for the dielectric maximum observed at −20–0°C as shown in Fig. 1(b). As shown in Fig. 1(a), the dielectric constants show typical relaxor-type frequency dependence at the ferroelastic phase transition. The lower the measurement frequency, the lower the temperature at which the phase transition appears. The resonance–antiresonance frequency for the present specimen was around 255 kHz, which is much higher than the frequency of 1 kHz used for characterizing ε_{33}^T. However, the piezoelectric anomaly appeared below the temperature of the dielectric maximum. Hence, this temperature discrepancy is not attributed to the difference in the measurement frequencies.

According to one pioneering study on SCNN single crystals,[8] SCNN shows two dielectric peaks at 100°C and –95°C when measured along ⟨001⟩ and ⟨110⟩, respectively, as well as a peak at 270°C for T_C. These dielectric peaks were attributed to the ferroelastic phase transition at 100°C and the loss of the polarizability along ⟨110⟩ at −95°C. Hence, the broad dielectric peak at −20–0°C observed for the randomly-oriented SCNN ceramics might be the result of a superposition of the two dielectric peaks at −95°C and 100°C, though it has been more simply understood as a ferroelastic phase transition. If this were the case, the temperature for the broad dielectric maximum may shift in accordance with the contributions from the two dielectric anomalies at 100°C and −95°C. Regarding the elastic property, it may be speculated that a larger elastic anomaly may occur at −95°C than at 100°C, so that the s_{11}^E maximum appears at a lower temperature than the temperature for the dielectric maximum.

Through the characterization of the temperature-dependent piezoelectric properties, it was shown that all the factors, k_{31}, ε_{33}^T, and s_{11}^E, increased in the vicinity of the ferroelastic phase transition to enhance the value of d_{31}. The remarkable improvement of d_{31} by 38% depicted in Fig. 1(b) was particularly driven by the increasing k_{31}. These results suggest that piezoelectric performance can be elevated by utilizing the ferroelastic phase transition.

Table 1. Longitudinal piezoelectric constants (d_{33}) and Curie temperatures reported for single crystals of typical tungsten bronze ferroelectrics[5),6),13),16)–19)]

Materials	T_C (°C)	d_{33} (pC/N)
$Sr_{0.6}Ba_{0.4}Nb_2O_6$	75, 75, 72, 75	180, 130, 130, 165
$Sr_{0.5}Ba_{0.5}Nb_2O_6$	128, 128, 118	110, 100, 90
$(Ba,Sr)Ti_2Nb_8O_{30}$	114	125
$Ba_2NaNb_5O_{15}$	560, 560, 560	37, 20, 37
$Ba_{2-x}Sr_xK_{1-y}Na_yNb_5O_{15}$	207	75
$Ba_{1.5}Sr_{0.5}K_{0.75}Na_{0.25}Nb_5O_{15}$	205	60
$Ba_{1.2}Sr_{0.8}K_{0.75}Na_{0.25}Nb_5O_{15}$	203	60
$Ba_{0.5}Sr_{1.5}K_{0.5}Na_{0.5}Nb_5O_{15}$	178, 170	80, 60
$Sr_{1.9}Ca_{0.1}NaNb_5O_{15}$	270	270
$Sr_2KNb_5O_{15}$	157, 150	95, 90
$K_3Li_2Nb_5O_{15}$	405	57
$Pb_2KNb_5O_{15}$	460	62
$Pb_{0.33}Ba_{0.70}Nb_{1.99}O_6$	350	60
$Pb_{0.37}Ba_{0.53}Nb_{2.04}O_6$	430	65
$Pb_{0.56}Ba_{0.44}Nb_{2.00}O_6$	315	185
$Pb_{0.6}Ba_{0.42}Nb_{1.99}O_6$	352	110
$Pb_{0.56}Ba_{0.4}Nb_{2.02}O_6$	367	140
$Pb_{0.6}Ba_{0.4}NbO_6$	350	100
$Pb_{0.86}Ba_{0.19}Nb_{1.98}O_6$	430	70

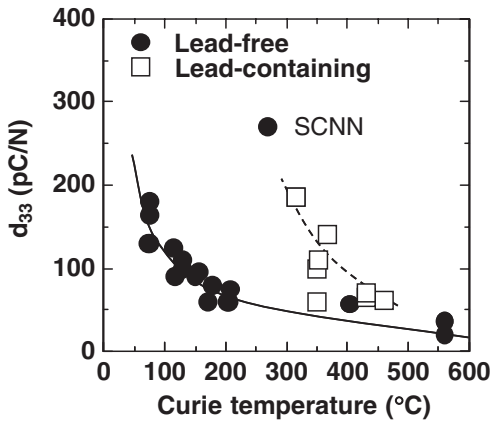

Fig. 2. Longitudinal piezoelectric constants (d_{33}) reported for single crystals of typical tungsten bronze ferroelectrics listed in Table 1 as a function of the Curie temperatures.

Based on the present results, it is expected that SCNN will show high piezoelectric performance at room temperature in spite of the high $T_C = 270$°C due to the ferroelastic phase transition close to room temperature. We summarize the relationship between d_{33} and T_C for various tungsten bronze crystals in **Table 1**.[5),6),13),16)–19)] **Figure 2** depicts the value of d_{33} of single crystals of typical tungsten bronze ferroelectrics listed in Table 1 as a function of T_C. As was reported for the perovskite ferroelectrics,[20] tungsten bronze crystals also follow this trade-off trend: the higher the value of T_C, the lower the value of d_{33}. Moreover, the lead-containing ferroelectrics always show a higher d_{33} if compared at the same T_C. In the figure, it is obvious that SCNN deviates from the trend curve. The d_{33} reported for SCNN is exceptionally high for the T_C. This specifically high d_{33} can be accounted for by the ferroelastic phase transition close to room temperature. This figure clearly depicts that a new lead-free tungsten bronze crystal, which has good piezoelectric perform-

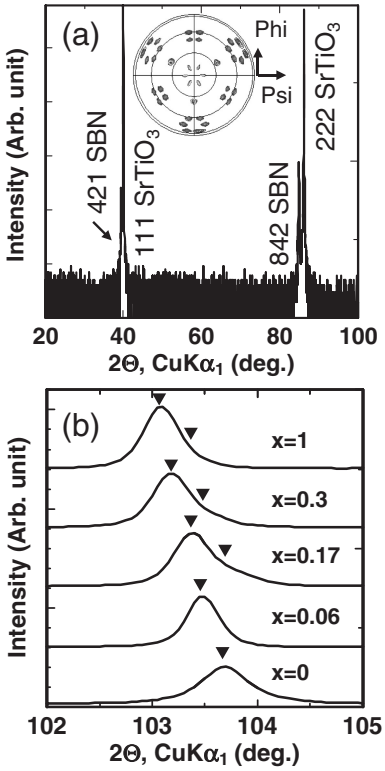

Fig. 3. (a) X-ray diffraction pattern of a $(421)_{tet}$-oriented epitaxial $(Sr_3Ba_2)Nb_{10}O_{30}$ film deposited on a (111)$SrTiO_3$ single crystal substrate. The inset is an X-ray polefigure measured for the $(421)_{tet}$-oriented $(Sr_3Ba_2)Nb_{10}O_{30}$ film under a fixed 2θ angle for 311_{tet} $(Sr_3Ba_2)Nb_{10}O_{30}$. (b) $900/090_{ortho}$ diffractions of the $(1-x)(Sr_3Ba_2)Nb_{10}O_{30}$–$xBa_4Bi_{2/3}Nb_{10}O_{30}$ epitaxial films. The triangles in the figure indicate the peak positions.

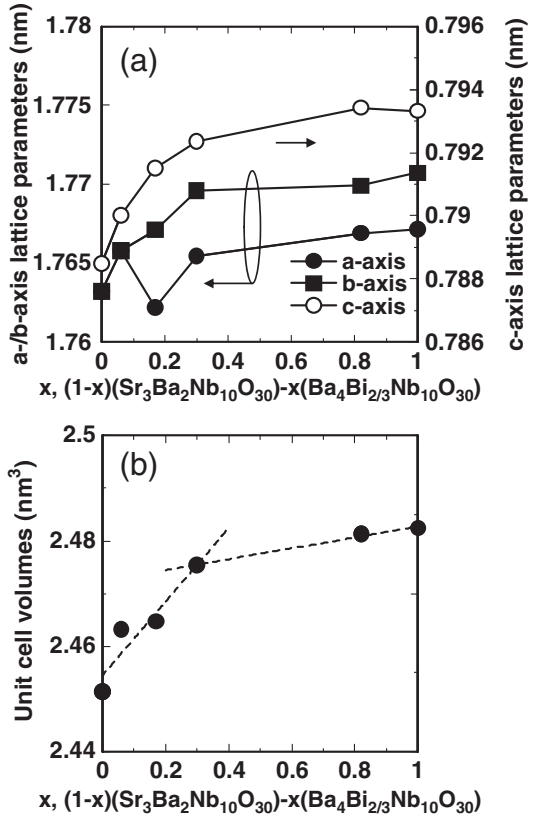

Fig. 4. (a) Lattice parameters and (b) unit cell volumes of the $(1-x)(Sr_3Ba_2)Nb_{10}O_{30}$–$xBa_4Bi_{2/3}Nb_{10}O_{30}$ epitaxial films.

ance comparable to that of lead-based crystals, could be produced by engineering the ferroelastic phase transition. Next, we investigated the composition-induced ferroelastic phase transition. The composition-induced ferroelastic composition is more attractive compared with the temperature-induced ferroelastic phase transition if high temperature stability is required for the piezoelectric performance.

3.2 Composition-induced ferroelastic phase transition

Ferroelastic phase transition as a function of the composition was investigated. **Figure 3**(a) shows the X-ray diffraction pattern for the SBN film deposited on a (111)$SrTiO_3$ substrate. In the 2θ–θ scan along the surface normal, only 421_{tet} and 842_{tet} SBN diffractions were confirmed for the film layer. The in-plane orientation and the $(421)_{tet}$ single orientation were confirmed by X-ray polefigures measured under a fixed 2θ angle for 311_{tet} SBN (see the inset in Fig. 3(a)). For this study, epitaxial $(421)_{tet}$-oriented $(1-x)$SBN–xBBN films ($x = 0$, 0.06, 0.17, 0.30, 0.82, and 1) were deposited. Every epitaxial film consisted of a single phase of the tungsten bronze structure.

To ascertain the phase transition composition between orthorhombic and tetragonal crystals, the lattice parameters were calculated from the positions of $900/090_{ortho}$ and 666_{ortho} diffractions given by X-ray asymmetric reflection measurements. As shown in Fig. 3(b), while the $900/090_{ortho}$ diffraction appeared as a single peak up to $x = 0.06$, it obviously split into two peaks for $x \geq 0.17$. On the other hand, the 666_{ortho} diffraction had no notable shoulder peak over the present composition range (not shown here). This peak split indicates that the a-axis and b-axis lattice parameters were no longer equal for $x \geq 0.17$, indicating the ferroelastic phase transition between the tetragonal and orthorhombic phases at $x = 0.06$–0.17. The calculated lattice parameters are summarized into **Fig. 4**(a).

The phase transition was cross-checked by tracking the change of the unit cell volumes induced by the compositional change. Figure 4(b) depicts the unit cell volumes calculated from the lattice parameters shown in Fig. 4(a). As the composition, x, increased, the cell volumes increased steeply up to $x = 0.3$, but moderately for $x \geq 0.3$ as shown in Fig. 4(b). This result supports the supposition that the crystal system undergoes a change with increasing x. Here, it should be mentioned that there is a discrepancy between the boundary compositions given by the lattice parameters and the unit cell volumes. This fact may imply that the two crystal phases coexisted in the vicinity of the boundary composition.[4] It can thus be deduced that the ferroelastic phase boundary between the tetragonal and orthorhombic crystal systems lies where $x = 0.06$–0.3.

The polarization and strain hysteresis loops were systematically measured at 80 K due to the low insulation resistance of the specimen at room temperature. **Figure 5**(a) depicts a representative polarization and strain hysteresis loops observed for the $(1-x)$SBN–xBBN film ($x = 0.17$) at 80 K. The coercive field and the remanent polarization were 47 kV/cm and 16 μC/cm^2, respectively. From the polarization hysteresis loops it was confirmed that all the films deposited for this study were ferroelectrics at 80 K.

The vertical strains of the samples when stressed with an electric field of about ±400 kV/cm were summarized with the

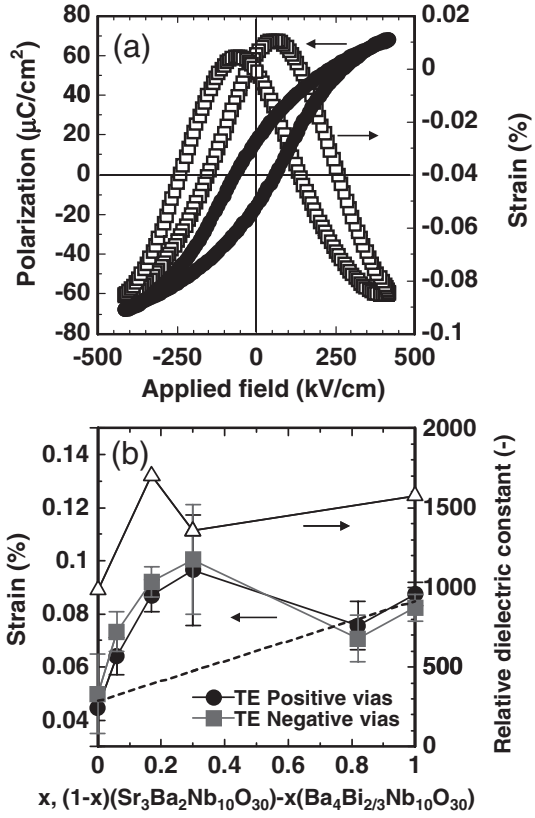

Fig. 5. (a) Polarization and strain hysteresis loops observed for the $(1-x)(Sr_3Ba_2)Nb_{10}O_{30}$–$xBa_4Bi_{2/3}Nb_{10}O_{30}$ epitaxial film ($x = 0.17$) at 80 K. The frequency of the applied triangular electric field was 100 kHz. (b) Strain under an electric field of ±400 kV/cm and the relative dielectric constants of the $(1-x)(Sr_3Ba_2)Nb_{10}O_{30}$–$xBa_4Bi_{2/3}Nb_{10}O_{30}$ epitaxial films measured at 80 K. For the relative dielectric constant measurements, a 1 MHz ac field with an amplitude of 50 mV was applied to the epitaxial films.

standard deviation as shown in Fig. 5(b). To assess the piezoelectric anomaly, a line (dashed line in the figure) that connects the average strains observed for the end-member crystals was drawn. As a result, it was found that the composition dependence of the electric field-induced strains is not straightforward, but has a broad strain maximum where $x = 0.17$–0.3. Although the phase boundary composition between the tetragonal and orthorhombic crystals at 80 K is not defined, the observed strain deviated from the linear line at the composition, for which the phase change was confirmed at room temperature. Furthermore, as can be seen in Fig. 5(b), the value of ε_r at 80 K had an anomaly in a quite similar fashion to the electric field-induced strains. Although the substrate bending effect emerged with the lateral piezoelectric strain[21),22)] could not be eliminated by, for example, a double laser interferometer, in the present strain measurements, there would be a piezoelectric anomaly at the ferroelastic phase transition of the $(1-x)$SBN–xBBN films.

4. Summary

The piezoelectric anomalies at the ferroelastic phase transition of lead-free tungsten bronze ferroelectrics were studied. First, the temperature-dependent piezoelectric anomalies in the vicinity of the ferroelastic phase transition of SCNN ceramics were characterized. At the phase transition temperature, every k_{31}, $\varepsilon_{33}{}^{T}$, and $s_{11}{}^{E}$ increased to enhance d_{31} by 38% compared with the room temperature value. Since SCNN has the ferroelastic phase transition close to room temperature, SCNN shows particularly good piezoelectric properties at room temperature for the high T_C. Second, the composition-induced ferroelastic phase transition was investigated for epitaxial films of $(1-x)$SBN–xBBN as a function of the composition. With careful X-ray diffraction analysis, it was found that the phase boundary between tetragonal and orthorhombic crystals lies where $x = 0.06$–0.3. The electric field-induced strain and the relative dielectric constants of the tungsten bronze ferroelectrics increased in the vicinity of the phase boundary at 80 K. It was concluded that engineering the ferroelastic phase transition is one approach to improving the piezoelectric properties of lead-free tungsten bronze ferroelectrics.

Acknowledgements This research was partially supported by Grants-in-Aid for Scientific Research and the Elements Science and Technology Project from the Ministry of Education, Culture, Sports, Science and Technology, Japan. The authors would like to thank Prof. S. Wada (Univ. of Yamanashi) for our valuable discussions.

References

1) B. Jaffe, W. R. Cook and H. Jaffe, "Piezoelectric Ceramics," Academic, New York (1971).
2) Y. Ishibashi and M. Iwata, *Jpn. J. Appl. Phys.*, **37**, L985–L987 (1998).
3) J. R. Oliver and R. R. Neurgaonkar, *J. Am. Ceram. Soc.*, **72**, 202–211 (1989).
4) M. Venet, F. L. Zabotto, J. A. Eiras and D. Garcia, *J. Appl. Phys.*, **105**, 124106 (2009).
5) R. R. Neurgaonkar, J. R. Oliver and W. K. Cory, *Ferroelectrics*, **160**, 265–276 (1994).
6) R. R. Neurgaonkar and W. K. Cory, *J. Opt. Soc. Am. B*, **3**, 274–282 (1986).
7) M. Kimura, T. Minamikawa, A. Ando and Y. Sakabe, *Jpn. J. Appl. Phys.*, **36**, 6051–6054 (1997).
8) R. R. Neurgaonkar, W. K. Cory and J. R. Oliver, *Mater. Res. Bull.*, **23**, 1459–1467 (1988).
9) R. R. Neurgaonkar, W. K. Cory, J. R. Oliver and M. Khoshnevisan, *Ferroelectrics*, **102**, 3–14 (1990).
10) R.-J. Xie, Y. Akimune, A. Matsuo and T. Sugiyama, *Appl. Phys. Lett.*, **80**, 835–837 (2002).
11) R.-J. Xie, Y. Akimune, R.-P. Wang and N. Hirosaki, *J. Am. Ceram. Soc.*, **85**, 2731–2737 (2002).
12) R.-J. Xie and Y. Akimune, *J. Mater. Chem.*, **12**, 3156–3161 (2002).
13) R. R. Neurgaonkar, J. R. Oliver and L. E. Cross, *Ferroelectrics*, **56**, 1035–1040 (1984).
14) T. Sugai, *Jpn. J. Appl. Phys.*, **26**, 778–779 (1987).
15) J.-K. Wang, N. Wakiya, K. Shinozaki and N. Mizutani, *J. Ceram. Soc. Japan*, **108**, 785–789 (2000).
16) T. R. Shrout, H. Chen and L. E. Cross, *Ferroelectrics*, **74**, 317–324 (1987).
17) R. R. Neurgaonkar, W. F. Hall, J. R. Oliver, W. W. Ho and W. K. Cory, *Ferroelectrics*, **87**, 167–179 (1988).
18) R. R. Neurgaonkar, W. K. Cory, J. R. Oliver, W. W. Clark, III, G. L. Wood, M. J. Miller and E. J. Sharp, *J. Cryst. Growth*, **84**, 629–637 (1987).
19) K. S. Rao and K. H. Yoon, *J. Mater. Sci.*, **38**, 391–400 (2003).
20) S. Zhang, R. Xia and T. R. Shrout, *J. Electroceram.*, **19**, 251–257 (2007).
21) K. Lefki and G. J. M. Dormans, *J. Appl. Phys.*, **76**, 1764–1767 (1994).
22) A. Barzegar, D. Damjanovic, N. Ledermann and P. Muralt, *J. Appl. Phys.*, **93**, 4756–4760 (2003).